CEAS Aeronautical Journal
https://doi.org/10.1007/s13272-026-00976-w

ORIGINAL PAPER

Effect of crashworthiness on the design of hydrogen aircraft

A. Medina Marrero[1] · M. F. M. Hoogreef[1] · P. Proesmans[1] · S. G. P. Castro[1]

Received: 24 October 2025 / Revised: 2 March 2026 / Accepted: 21 May 2026

Abstract

Hydrogen aircraft are strong candidates in the fight to reduce climate emissions in aviation. The main challenge in designing hydrogen aircraft lies in the storage of hydrogen, which requires four times more volume compared to kerosene alternatives. Furthermore, to ensure crashworthiness, it is desirable to prevent damage to the hydrogen tank during a crash landing by reducing its diameter via the crashed diameter coefficient. This requires a longer tank, which snowballs into larger, less efficient aircraft. The objective of this research is to quantify the effect of the crashed diameter coefficient on aircraft performance. This has been done by modifying a hydrogen aircraft design framework to include crashworthiness and performing multidisciplinary design optimizations that minimize mission energy. Additionally, a number of design variables were varied to study how different design parameters affect the tendencies, such as changing the span limit, seats abreast or the payload-range requirement. It was found that accounting for the crashed diameter coefficient can increase the fuselage length and maximum take-off mass by 17% and 6%, respectively, for a medium range aircraft like the Airbus A320. Alternatively, if the length of the fuselage is kept fixed, a 20% reduction in payload or a 60% reduction in range would be required. Overall, it has been found that crashworthiness needs to be considered in the preliminary stage of hydrogen aircraft design.

Keywords Aircraft design · Hydrogen aircraft · Crashworthiness · Multidisciplinary design optimization

Abbreviations

LH_2	Liquid hydrogen
BASE	Baseline aircraft, with no modifications
BPR	Bypass ratio
DPAY	Aircraft with modified payload requirement compared to BASE
DRANG	Aircraft with modified design range requirement compared to BASE, whilst proportionally modifying the ferry range
FW	Framework
HPC	High pressure compressor
LHV	Lower heating value [J/kg]
LPC	Low pressure compressor
MDO	Multidisciplinary design optimization
MED	Medium-range aircraft, based on Airbus A320
MTOM	Maximum take-off mass
OEI	One engine inoperative
OEM	Operating empty mass
OPR	Overall pressure ratio
OVER	'Over-sized' aircraft; a larger aircraft category (with more seats abreast) performing the mission of a smaller aircraft category
REG	Regional-type aircraft, based on Embraer E175
SEC	Specific energy consumption [MJ/(Ns)]
SPAN	Relaxed span limit on BASE aircraft
TET	Turbine entry temperature [K]
TLAR	Top-level aircraft requirements
TSFC	Thrust specific fuel consumption [kg/(Ns)]
XDSM	Extended design structure matrix

List of symbols

$(h/r)_{\text{dome}}$	Ratio between the tank dome height and the tank radius [–]
β_{crash}	Crashed diameter coefficient [–]
η_{grav}	Gravimetric efficiency of hydrogen tank [–]
η_{ov}	Overall propulsion efficiency [–]
λ	Taper ratio [–]
$\Lambda_{0.25}$	Wing quarter-chord sweep [deg]

✉ S. G. P. Castro
S.G.P.Castro@tudelft.nl

[1] Faculty of Aerospace Engineering, Delft University of Technology, 2629 HS Delft, The Netherlands

Published online: 09 June 2026

g	Constraint vector
x	Design vector
$\overline{V}$	Tail volume coefficient [−]
Π	Pressure ratio [−]
ρ	Density [kg/m^3]
A	Wing aspect ratio [−]
b	Wing span [m]
C_D	Drag coefficient [−]
C_L	Lift coefficient [−]
d	Diameter [m]
D_{fus}	Fuselage diameter [m]
e	Oswald efficiency factor [−]
f_W	Landing mass factor [−]
$f_{V,\text{extra}}$	Extra volume allowance of hydrogen tank [%]
h	Altitude [m]
M	Mach number [−]
m	Mass [kg]
r	Range or radius [km or m]
S	Wing surface area [m^2]
s	Distance [m]
T	Thrust [N]
t_{bl}	Block time [h]
V_{tank}	Tank volume [m^3]
W	Weight [N]

Sub- and superscripts

*	Optimal solution
0	Sea-level condition or initial value
0.25	Measured at quarter-chord
afse	Airframe systems and equipment
app	Approach condition
bl	Block mission parameter
cr	Cruise condition
eng	Engine
fus	Fuselage
harm	Harmonic
ht	Horizontal tail
L	Lower bound
ops	Operations
pol	Polytropic
TO	Take-off condition
U	Upper bound

1 Introduction

Aviation's climate impact in 2011 was estimated to be responsible for 3.5% of anthropogenic emissions [1], and by 2050, carbon dioxide emissions from aviation are expected to double compared to the year 2000 [2]. To meet the climate goals set by many countries, drastic measures are required across all areas of aviation, from operations to the development of new technologies. This context has renewed interest in alternative fuels and propulsion concepts that can enable a sustainable future for aviation.

Hydrogen has emerged as a promising solution for significantly reducing aviation emissions. When used as a fuel, whether burned in modified gas turbines or converted to electricity via fuel cells, hydrogen yields no direct CO_2 emissions; low or zero NO_x in combustion and fuel cells, respectively [3]. In terms of energy content, hydrogen offers a gravimetric energy density around three times higher than conventional Jet-A kerosene [4, 5] ($\sim$120 MJ/kg versus $\sim$ 43 MJ/kg), meaning far less fuel mass is required for a given mission. These attributes make hydrogen an attractive candidate for aviation's decarbonization [3, 6].

However, hydrogen's advantages come with large systemic challenges. Liquid hydrogen (LH_2), requires four times as much volume as compared to kerosene for the same amount of stored energy [7], and it is important to mention that this does not include the volumes of all associated thermal insulation and cryogenic systems [8]. LH_2 is the only viable option for hydrogen storage on long-range aircraft, providing the lightest tanks and highest energy density necessary to address mass and volume limitations [9]. Out of all proposed tank integration options, including overhead tanks [4, 8, 10, 11] and wing podded [12], the most researched options are tanks in the fuselage [4, 13–19], or tanks in the main body of the aircraft for blended wing-body designs [3, 20, 21]. Studies show that for energy-optimal aircraft, compared to the kerosene counterpart, LH_2 aircraft have a 6% increase in OEM, 16% increase in fuselage length and a 4% decrease in lift-to-drag [22].

Current models likely overestimate the allowable tanks size and hydrogen fuel quantity, pointing an overly optimistic picture of aircraft performance and range. None of the aforementioned studies designing hydrogen-powered aircraft considered constraints related to the behavior of the airframe under controlled crash scenarios, such as emergency landing. The airframe significantly deforms under such scenarios, and in the present study we refer to this overall deformation as the crashworthiness performance of the airframe. There are many safety hazards associated with LH_2 systems for commercial aviation due to its high flammability. Via a preliminary safety assessment, Simonetto et al. [23] identified damage to the LH_2 system due to a collision or crash as one of the most significant risks. It is evident that in the event of a crash landing, damage to the LH_2 system would be catastrophic. Current conceptual studies generally assume that any available volume inside the fuselage can be utilized for LH_2 storage, effectively ignoring its crashworthiness performance.

For conventional aircraft, the evaluation of crashworthiness is commonly performed relatively late in the design process, typically left until after static sizing [24], involving detailed models that already contain specifics about the layout of primary structural elements such as frames, stringers, skin, cross beams and so forth. However, for LH_2 aircraft it is expected that the crashworthiness performance directly influences the amount of hydrogen that can be stored in a given fuselage configuration, becoming a constraint that is coupled with the aircraft performance and sizing.

The present study is the first to quantitatively include crashworthiness in the preliminary design of hydrogen-powered aircraft, by adopting a design philosophy to prevent damage to the LH_2 systems, while removing the simplification to fill the entire fuselage cross-section with a hydrogen tank that is adopted by current studies. This philosophy is a conservative choice aligned with the recognition that the crashworthiness behavior of large LH_2 tanks is not well characterized [25]. The basic idea is to allow sufficient crashworthiness performance of the fuselage airframe to attain enough crushing distance before the crash deformations reach the hydrogen tank.

This manuscript is structured as follows. Section 2 describes the optimization framework, how crashworthiness is accounted for in a conceptual aircraft design library, and the different cases that are going to be analyzed in section 4. Before that, section 3 describes the verification of the aircraft design library with crashworthiness. A review of the assumptions involved in the hydrogen tank design is performed with sensitivity studies in section 5. Finally, section 6 presents the conclusions and recommendations.

2 Methodology

2.1 Crashed diameter coefficient

The ability of a fuselage structure in absorbing the energy of the crash can be modeled by the crashed diameter coefficient (or simply the crash coefficient) β_{crash} [26]. It is defined equivalently by Eq. (1) or Eq. (2), where D stands for diameter and A for cross-sectional area, with the latter definition allowing for non-cylindrical fuselages. The coefficient quantifies the available crushing stroke of the airframe, and dictates the maximum cross-section available for critical components, such as the LH_2 system, to ensure the deformation zone does not spatially intersect these components and thus prevents catastrophic damage during a crash landing.

$$\beta_{\text{crash}} = \frac{D_{\text{crash}}}{D_{\text{fus}}} \tag{1}$$

$$\beta^2_{\text{crash}} = \frac{A_{\text{crash}}}{A_{\text{fus}}} \tag{2}$$

The definition of the crashed diameter coefficient can be exemplified via the A320 fuselage drop test [27] shown in Fig. 1. With this figure, the crashed diameter coefficient of the A320 fuselage can be approximated by measurement; $D_{\text{crash}} = 2.62$ m and $D_{\text{fus}} = 3.95$ m, yielding $\beta_{\text{crash}} = 0.663$.

Fuselages with large crash coefficients are efficient in absorbing the energy of the crash, and hence have relatively small crushing distances. This allows a large proportion of the fuselage cross-section to be utilized for critical components such as the hydrogen tank. Large crash coefficients are desirable as to increase the usable cross-section area of the fuselage.

By definition, using the crashed diameter coefficient in the design prevents tank rupture, which is the primary defence against catastrophic fuel release. However, in relation to crashworthiness requirements, this metric does not represent occupant injury criteria, such as the dynamic response index (DRI), head injury criterion (HIC), or lumbar loads. Furthermore, the coefficient does not explicitly account for post-crash fire mechanisms related to inertial failures (e.g. rupture of fuel lines) or evacuation path maintenance (e.g., significant damage on the cabin floor or door frame deformation), relying instead on the assumption that tank-structure geometric separation is a fundamental prerequisite for guaranteeing passenger safety during and after a crash.

Although β_{crash} has been accounted before for the design of hydrogen-powered eVTOLs [26], the effect of the crashed diameter coefficient on aircraft performance has not yet been studied. Reducing the diameter of the hydrogen tank in accordance with β_{crash} for the same payload and range would require a larger fuselage, snowballing into a heavier and potentially more costly aircraft. The precise extent to which this would occur remains to be determined, being the focus of the present study.

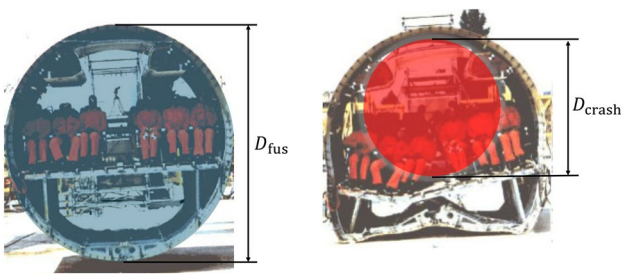

Fig. 1 A320 drop test, modified from LePage [27]. On the left is the fuselage pre-crash and on the right post-crash

2.2 Optimization problem formulation

A multidisciplinary design optimization (MDO) is used to design energy-optimal aircraft for an assumed value of the crashed diameter coefficient. Then, as β_{crash} is varied, the associated aircraft can be compared and the effect of crashworthiness can be quantified. The aircraft design library that performs the complete aircraft conceptual sizing is based on Proesmans and Vos (2024) for hydrogen aircraft [22], but modified with the addition of β_{crash}. This section addresses firstly the optimization formulation in subsection 2.2. Then, the modifications on Proesmans' framework are explained in subsection 2.3 and finally in subsection 2.4 the different scenarios that will be considered are introduced. These scenarios aim to identify key parameters that can be used to control or reduce the effect of the crash coefficient. The MDO problem definition is based on that of Proesmans and Vos [22], and is defined as follows:

$$
\begin{aligned}
\underset{\mathrm{x}}{\text{minimize}} \quad & F(\mathrm{x}) = E_{\text{fuel}}(\mathrm{x}) \\
\text{subject to} \quad & W/S \leqslant \tfrac{1}{2}\rho_0 \left(\frac{v_{\text{app}}}{1.23}\right)^2 C_{L_{\max}} / f_W \\
& b \leqslant b_{\max} \\
& \text{TET}_{\text{TO}} \leqslant \text{TET}_{\text{TO,max}} \\
& \text{OPR}_{\text{cr}} \leqslant \text{OPR}_{\text{cr,max}} \\
& C_{L_{\text{cr}}} \leqslant \frac{C_{L_{\text{buffet}}}}{1.3} = \frac{0.86 \cdot \cos \Lambda_{0.25}}{1.3} \\
& x_i^L \leqslant x_i \leqslant x_i^U \qquad \text{for } i = 1, 2, \ldots, 9
\end{aligned}
\tag{3}
$$

The objective of the optimization problem is to minimize the mission energy E_{fuel}, which is equivalent to minimizing the fuel mass m_{fuel}, by varying the nine design variables that comprise the design vector x. These variables are related to the airframe, engines, and mission, and are summarized in Table 1 with their bounds [22]. These design variables are selected to control key conceptual design decisions and offer a large design space, while limiting the size of the design vector. The wing planform is controlled through the wing aspect ratio, wing loading, and Mach number. Planform parameters such as sweep angle, taper ratio, and thickness-to-chord ratio are derived from conceptual design rules [28, Appendix C]. The engine design variables determine the on-design thermodynamic cycle in cruise conditions, which are in turn set by the cruise Mach number and altitude design variables.

Table 1 Design variables and their respective bounds, from Reference [22]

Variable	Description [unit]	Lower bound (x^L)	Upper bound (x^U)
W/S	Wing loading [kN/m^2]	3.00	6.50
A	Wing aspect ratio [–]	7.00	12.0
BPR	Bypass ratio in cruise [–]	6.00	11.0
Π_{fan}	Fan pressure ratio in cruise [–]	1.30	1.80
Π_{lpc}	LPC pressure ratio in cruise [–]	1.20	1.80
Π_{hpc}	HPC pressure ratio in cruise [–]	15.0	25.0
TET	Turbine entry temperature in cruise [K]	1350	1700
h_{cr}	Initial cruise altitude [km]	6.00	12.0
M_{cr}	Cruise Mach number [–]	0.50	0.90

The four constraints are collectively grouped by g, and define limits for parameters related to the geometry, engine performance, and aerodynamics that are directly influenced by the design variables and that could not be readily implemented through conceptual design rules [28]. The first constraint ensures that the wing loading is compatible with the approach speed v_{app}, which is given as a Top-Level Aircraft Requirement in subsection 2.4. The second constraint limits the span to the maximum allowed within a specific ICAO category. The third and fourth constraint restrict the maximum turbine entry temperature at take-off (ISA+15) and the overall pressure ratio at the top-of-climb to 2000 K and 60, respectively [28]. The final constraint prevents the buffet onset condition, via the lift coefficient in cruise. The mission energy is evaluated at the harmonic point, as further explained in subsection 2.4.

Figure 2 shows the structure of the MDO in the format of an extended design structure matrix. An optimization algorithm feeds the design vector to the convergence loop that performs the complete aircraft conceptual sizing. Once the aircraft is converged to 0.01% of the operating empty mass (OEM), the constraints are evaluated. The convergence iterations consist of three main disciplines, each composed of smaller modules [22, Section 2.2]. The airframe discipline, that is expanded in Fig. 3, performs a Class-I sizing, builds the quadratic drag polar, and estimates the OEM of the aircraft based on Class-II component weight estimations. In the Class-I sizing step, the minimum thrust-to-weight ratio (T_{TO}/W) is selected which meets the take-off, cruise speed, cruise altitude, and CS25 climb gradient constraints (take-off path, aborted landing, OEI take-off and OEI approach), for the wing loading selected by the optimize and limited by the approach speed.

The drag polar and thrust from this first module are used to thermodynamically size the turbofan and perform off-design analyses. The latter provide the necessary inputs to determine the conceptual geometry and mass of the turbofan engines and the nacelles. This airframe discipline also determines the location of the wing that minimizes the size of the horizontal tail, considering the center-of-gravity excursion and longitudinal stability and trim conditions [22]. The outputs from the airframe discipline, together with engine parameters, are fed to a mission analysis based on the conceptual lost-range method [29]. This analysis provides an update of the harmonic fuel mass $m_{\text{fuel,harm}}$. The OEM and $m_{\text{fuel,harm}}$ estimates are used to re-evaluate the MTOM and continue until the design parameters converge.

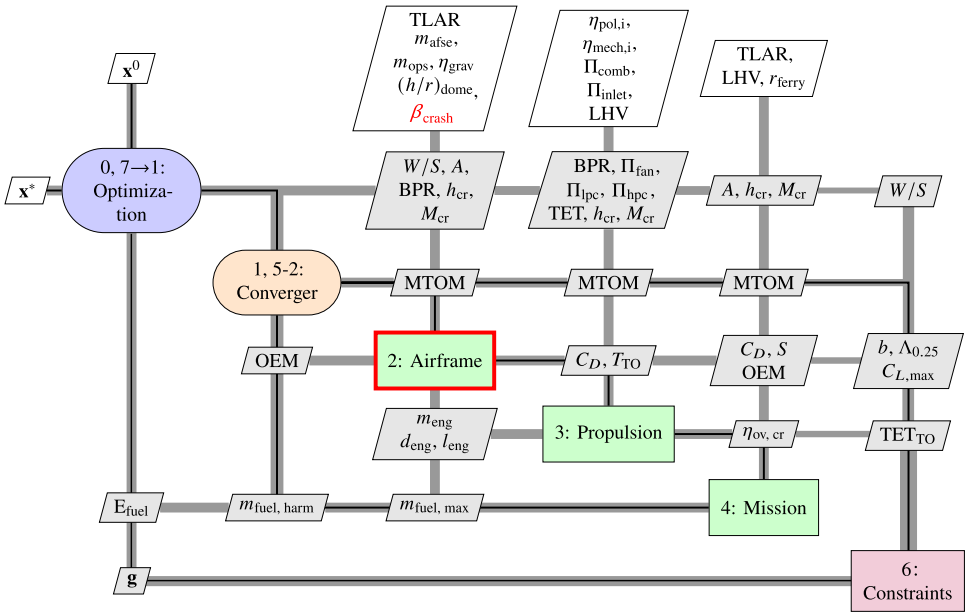

Fig. 2 Extended design structure matrix, adapted from [22]. Modifications are shown in **red**

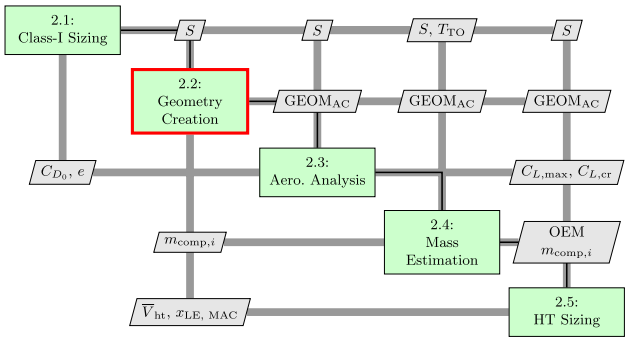

Fig. 3 Airframe design and analysis workflow (step 2 of workflow in Fig. 2), adapted from [22]. Modifications are shown in **red**

2.3 Changes to framework - hydrogen tank sizing with crashworthiness

The modifications made to the design framework of Proesmans and Vos [22] are highlighted in red in Figs. 2 and 3. The crashed diameter coefficient (β_{crash}) is imposed externally, and it only influences the airframe sizing module via the hydrogen tank sizing in the geometry creation routine. The hydrogen tank is modeled as a cylindrical non-integral tank behind the cabin [22]. Three hyper-parameters drive the tank geometry and weight:

- $(h/r)_{\text{dome}}$, the ratio between dome height and tank radius. It affects the length and mass of the tank, but the latter is not accounted for in the model. It is taken to be 0.3.[22]
- $f_{V,\text{extra}}$, extra volume allowances. It accounts for contraction and expansion, ullage, internal equipment and trapped fuel, but it does not account for boil-off. It is taken at 3.8% [22]
- $\eta_{\text{grav}} = m_{\text{fuel}}/(m_{\text{fuel}} + m_{\text{tank}})$, gravimetric index. It is taken at 0.773 [18].

Given the maximum fuel mass $m_{\text{fuel,max}}$ obtained from the ferry range r_{ferry}, and the density of LH_2 ($\rho_{LH_2} = 71\,\text{kg/m}^3$), the maximum tank volume V_{tank} can be obtained via Eq. (4).

$$V_{\text{tank}} = \frac{m_{\text{fuel,max}}}{\rho_{LH_2}}(1 + f_{V,\text{extra}}) \tag{4}$$

The length of the tank l_{tank} is computed by Eq. (5).

$$l_{\text{tank}} = \frac{1}{\pi r_{\text{tank}}^2}\left[V_{\text{tank}} - \frac{4\pi}{3} r_{\text{tank}}^2 h_{\text{dome}}\right] + 2h_{\text{dome}} \quad \text{where } h_{\text{dome}} = r_{\text{tank}} \cdot (h/r)_{\text{dome}} \tag{5}$$

And finally, the radius of the hydrogen tank r_{tank} is modified as shown in Eq. (6).

$$r_{\text{tank}} = D_{\text{fus,inner}}/2 \xrightarrow{\text{crashworthiness}} r_{\text{tank}} = \beta_{\text{crash}} D_{\text{fus,outer}}/2 \tag{6}$$

In the above, $D_{\text{fus,inner}}$ and $D_{\text{fus,outer}}$ are the fuselage inner and outer diameters, respectively. The difference $\Delta D = D_{\text{fus,outer}} - D_{\text{fus,inner}}$ accounts for insulation and structural components, and is constant for the aircraft category in question. It can be seen that in Proesmans' framework, by default, the aircraft is designed with a usable diameter that is equivalent to the following crashed diameter coefficient:

Table 2 Top-Level Aircraft Requirements of BASE [30, 31]

Requirement [unit]	Regional [REG]	Short/ medium range [MED]
Maximum structural payload $m_{\mathrm{pl,max}}$ [metric tons]	10.1	18.2
Harmonic range r_{harm} [km (nm)]	2410 (1300)	3200 (1730)
Ferry range r_{ferry} [km (nm)]	4630 (2500)	6750 (3645)
Approach speed v_{app} [m/s (kts)]	69.0 (134)	70.0 (136)
Take-off length (ISA SL conditions) [m (ft)]	1700 (5580)	2100 (6890)
ICAO Reference Code	3C	4C
Maximum span b_{max} [m]	36.0	36.0
Diversion range r_{div} [km (nm)]	185 (100)	463 (250)
Loiter time t_{hold} [min]	45	35
Landing mass factor f_W [-]	0.97	0.94
Seats abreast n_{abreast} [-]	4	6

$$\beta_{\mathrm{max}} = \frac{D_{\mathrm{fus,inner}}}{D_{\mathrm{fus,outer}}} \tag{7}$$

For narrow-body aircraft, $\Delta D = 15\,\mathrm{cm}$ [28]. Therefore, for a six-abreast configuration $\beta_{\mathrm{max}} \approx 0.963$, whilst for a four-abreast configuration $\beta_{\mathrm{max}} \approx 0.950$. The symbol has been given the subscript max as any higher β_{crash} would be incompatible with a non-integral tank.

In the present work, the mass of the crashworthiness structure that would ensure a given crash coefficient has not been accounted for in the mass of the fuselage, such that changes in fuselage mass are mainly due to changes in fuselage length associated with the different crash coefficients. This limitation is further discussed in subsection 4.6.

2.4 Top-level aircraft requirement cases

This study focuses on two main aircraft categories; regional (REG) and short/medium-range (MED) aircraft. Top-Level Aircraft Requirements (TLAR) for the baseline (BASE) aircraft are given in Table 2. The values are based on the Embraer E175 [30] and Airbus A320 [31] for the regional and short/medium-range aircraft, respectively.

Starting from these 'BASE' aircraft, a number of deviations are considered with the aim of evaluating how other design parameters play a role in the sensitivity of β_{crash}. In this study, four cases are considered; the effect of the maximum span limit, the number of seats abreast, and changes to the payload and range requirements.

1. SPAN: to evaluate the effect of a larger wing span. This option relaxes the span constraint to the next ICAO gate category. For both REG and MED aircraft, this is 42 m.
2. OVER: "over-sized" option, to study (mainly) the effect of the seats abreast. This is done by having a MED aircraft perform the mission of the REG aircraft. The resulting aircraft's TLAR are a combination of the REG and MED aircraft; it has the maximum structural payload, harmonic range, and ferry range of the REG aircraft, and the rest of the parameters from the MED aircraft category.
3. DPAY: to evaluate the effect of changing the payload requirement. This option varies the maximum structural payload by a factor $f_{\mathrm{pay}} \in [0.25, 1.4]$. From this payload mass, the number of passengers is computed from the maximum number of rows that can be filled. The extra mass is considered as cargo mass.
4. DRANG: to evaluate the effect of changing the range requirement. This is done by varying both the harmonic range and the ferry range by a factor $f_{\mathrm{rang}} \in [0.25, 1.4]$.

Table 3 Deviations of Top-Level Aircraft Requirements from BASE. The symbol '=' refers that the TLAR is equal to that of the category of aircraft it refers to; i.e. REG SPAN has a v_{app} associated to the REG category

Requirement [unit]	BASE	SPAN	OVER	DPAY	DRANG
Maximum structural payload $m_{\mathrm{pl,max}}$ [metric tons]	=	=	REG	$\times f_{\mathrm{pay}}$	=
Harmonic range r_{harm} [km (nm)]	=	=	REG	=	$\times f_{\mathrm{rang}}$
Ferry range r_{ferry} [km (nm)]	=	=	REG	=	$\times f_{\mathrm{rang}}$
Approach speed v_{app} [m/s (kts)]	=	=	MED	=	=
Take-off length (ISA SL conditions) [m (ft)]	=	=	MED	=	=
ICAO Reference Code	=	↑	MED	=	=
Maximum span b_{max} [m]	=	↑	MED	=	=
Diversion range r_{div} [km (nm)]	=	=	MED	=	=
Loiter time t_{hold} [min]	=	=	MED	=	=
Landing mass factor f_W hydrogen [-]	=	=	MED	=	=
Seats abreast n_{abreast} [-]	=	=	MED	=	=

The relationship between the deviation studies and the top level aircraft requirements can be found in Table 3.

The reason why RANG specifies changes to r_{ferry} stems from how the hydrogen tank is sized (refer to subsection 2.3). The maximum fuel capacity is determined by the ferry range. Thus, if the effect of varying the design range is to be studied, the ferry range needs to be considered in some way. In this study, it is assumed that r_{ferry} varies proportionally with r_{des}. This ensures that $r_{\mathrm{ferry}}/r_{\mathrm{des}}$ remains constant,

implying that the same relative fuel mass is used for the ferry range independently of f_{rang}.

3 Verification

The verification of the aircraft design framework (FW) for conventional kerosene-based aircraft has been discussed in earlier research [28, 32]. These previous verification steps concluded that the design modules can estimate the mass and geometry parameters of regional aircraft (Embraer 175 [30]) and medium-range aircraft (Airbus A320 [31]) with −4.2% to +2.5% accuracy. The framework tends to underestimate the masses by up to −1.6% for both aircraft. Geometry parameters on the other hand are overestimated for the A320 and underestimated for the E175.

The remainder of this section aims to verify the implementation of the crashed diameter coefficient that is explained in section 2. The verification is performed by comparing the current framework after the implementation of β_{crash}, with the energy-optimal MED aircraft of Proesmans and Vos (2024). To verify the framework with the coefficient implemented, the crashed diameter coefficient is set at $\beta_{\max} = 0.963$. As discussed in subsection 2.3, this value for a MED six-abreast aircraft causes the diameter of the hydrogen tank to be equal to the inner fuselage diameter, and hence is equivalent to the results of the previous implementation without crashworthiness considerations.

The verification process is divided into two distinct stages to decouple the evaluation of the objective function (the aircraft synthesis routine) from the optimization algorithm. Referring back to Fig. 2, the converger (1,5-2) is treated separately from the optimization (0,7-1).

First, to verify changes on the aircraft synthesizer, the different frameworks are compared using the same input design vector. This design vector is composed of the optimized design variables from Proesmans and Vos [22] that minimize mission energy; these are shown in the first column of Table 5. In the second column, the results of the current framework setting $\beta_{\text{crash}} = 0.963$ are shown. Overall, looking at the right side of Table 4, it can be concluded that the implementation of β_{crash} has been done correctly, as no changes can be observed in any of the parameters. Hence, with the implementation of the crashed diameter coefficient, the objective function evaluates to the same value of mission energy.

On the other hand, the optimized design variables to minimize mission energy are compared in Table 5. From the previous discussion, the differences between the two are only attributed to the different optimization algorithms used, as the objective function renders the same numerical value. Proesmans used an implementation of the Nelder-Mead Simplex algorithm in the software modeFRONTIER with two termination criteria (termination accuracy of 1×10^{-5} and a maximum number of function evaluation of 2000 [22]). The current implementation uses the SLSQP algorithm implemented in SciPy with the default termination criteria [33]. In this particular execution, the starting point was set at the optimum from Proesmans and Vos [22]. Overall, these discrepancies show that the current optimizer converges to a different optimum, with a slightly better objective function value. It is interesting to note that the current optimization setup favors the upper bound of wing aspect ratio and the bypass ratio.

Table 4 Verification of the aircraft design convergence, using design variables from Table 5 in [22] for the energy-optimal LH_2 MED aircraft

Parameter [unit]	Proesmans (2024) [22]	FW with $\beta_{\text{crash}} = 0.963$	Diff. [%]
MTOM [metric tons]	64.5	64.5	+0.0
OEM [metric tons]	42.8	42.8	+0.0
S [m^2]	115	115	+0.0
b [m]	36.0	36.0	+0.0
$\Lambda_{0.25}$ [deg]	18.0	18.0	+0.0
λ [-]	0.310	0.310	+0.0
l_{fus} [m]	43.5	43.5	+0.0
S_{ht} [m^2]	38.9	38.9	+0.0
$(L/D)_{\text{cr}}$ [-]	18.4	18.4	+0.0
$(T/W)_{\text{TO}}$ [-]	0.303	0.303	+0.0
T_{TO} [kN]	192	192	+0.0
TSFC_{cr} [10^{-5}kg/(N s)]	0.5	0.5	+0.0
$\eta_{\text{ov,cr}}$ [%]	38.6	38.6	+0.0
SEC_{cr} [10^{-4}MJ/(N s)]	5.52	5.52	+0.0
Energy [MJ/(pax km)]	0.57	0.57	+0.0
t_{bl} [h]	5h22m	5h22m	+0.0
$N_{\text{AC,max}}$ [10^3]	15.2	15.2	+0.0

Table 5 Verification of implementation of crash diameter coefficient; comparison of MED aircraft optimized for mission energy

Parameter [unit]	Proesmans (2024) [22]	FW with $\beta_{\text{crash}} = 0.963$	Diff. [%]
A [-]	11.3	12.0	+6.4
W/S [kN/m^2]	5.50	5.34	−2.9
BPR [-]	9.77	11.00	+12.6
Π_{fan} [-]	1.70	1.63	−4.4
Π_{lpc} [-]	1.50	1.57	+4.8
Π_{hpc} [-]	22.3	23.4	+5.0
TET [10^3 K]	1.47	1.48	+0.7
h_{cr} [km]	10.8	11.0	+2.0
M_{cr} [-]	0.720	0.735	+2.2
Energy [MJ/(pax km)]	0.57	0.56	−2.4

4 Results and discussion

In this section, the optimizations are performed, as described in section 2, for the different cases given in subsection 2.4. Firstly, the BASE aircraft is studied. Then the SPAN and OVER cases are investigated, followed by DPAY and DRANG. This section concludes with the limitations of the present framework.

4.1 BASE aircraft

The trends of the crashed diameter coefficient against important aircraft performance parameters are discussed for energy-optimal MED aircraft, and then REG aircraft. Figure 4 shows the deviations of the parameters with respect to the $\beta_{\text{crash}} = 0.963$ aircraft, for the MED BASE case.

It can be seen that as the crash coefficient is reduced, the fuselage dramatically increases in length, up to 48% longer compared to that of $\beta_{\text{crash}} = 0.963$, due to the increased length of the hydrogen tank that is needed to accommodate the smaller crashworthy diameter. Furthermore, the wing loading remains constant at its maximum feasible value for all β_{crash}. Since the wing loading is constant and the MTOM increases, so must the wing surface area by the same amount. The wing aspect ratio has to decrease to not exceed the wing span limits, wing span which remains at its upper bound for all β_{crash}. This decrease in aspect ratio causes a poorer climb gradient performance, which increases the thrust loading. Notice how the cruise altitude, OPR, BPR and TET show invariance with β_{crash} for the MED BASE aircraft. The jump in TET at $\beta_{\text{crash}} = 0.85$ is likely numerical noise in the optimization. Compared to the $\beta_{\text{crash}} = 0.963$, when the crash coefficient is reduced to 0.663 the MTOM and mission energy experience increases of 6% and 9%, respectively.

With the same dataset of baseline MED aircraft, different deviations are obtained when setting a different reference point. When $\beta_{\text{crash}} = 0.663$ is set as such a reference point, the graph can be used to estimate the improvement or reduction of the aircraft performance when the crash coefficient is increased or decreased from the value of the A320, as seen in Fig. 5. The resulting geometries are better visualized when plotting the geometry against the A320 top view in Fig. 6.

In Table 6, a mass breakdown of the OEM is included for selected MED BASE aircraft with different crashed diameter coefficients. As expected, changes in β_{crash} have the greatest impact on the fuselage mass, which drives most of the variation in OEM. However, these results only reflect the geometric effects of the crashed diameter coefficient; additional mass required for the crashworthiness structure is not accounted for in the Class II weight estimation. This limitation is further discussed in subsection 4.6.

For energy-optimal REG aircraft, the trends are different, as shown in Fig. 7. The most noticeable change is that now the span is not limiting, but the wing aspect ratio is. The optimizer chooses to decrease the wing loading as the crash coefficient is reduced. Since the take-off constraint is limiting in the thrust-loading versus wing-loading diagrams (refer to Appendix A.1), this explains why the thrust loading curve also decreases with a similar trend. The reason that both curves don't intersect exactly for lower crash coefficients hinges on the effect of the cruise speed. As the cruise speed is reduced, the sweep angle also decreases, which increases the landing $C_{L,\max}$. This relaxes both the landing and take-off constraints in the constraint diagram, but only the latter is active. Consequently, as the wing-loading is simultaneously reduced, the thrust-loading decreases even further. As a consequence of a smaller wing loading and a larger MTOM, the wing surface must increase, and since the wing aspect ratio remains constant, the span also increases.

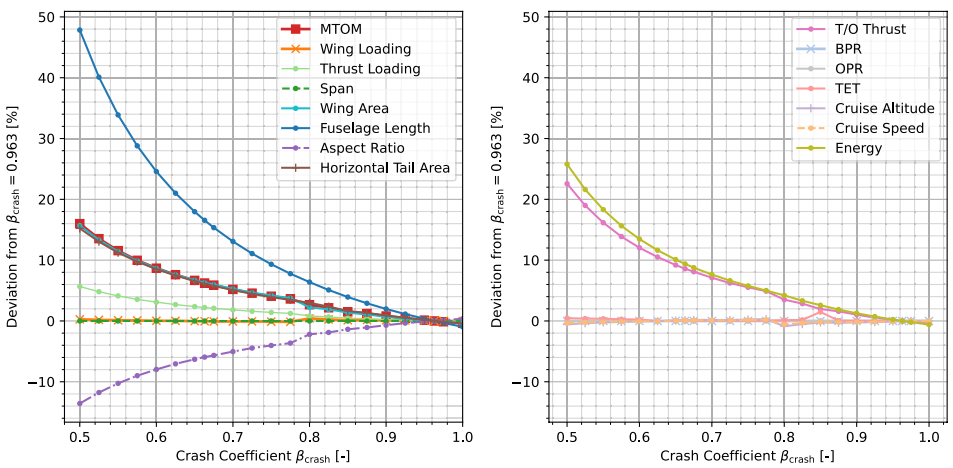

Fig. 4 Deviations of MED BASE aircraft with respect to that at $\beta_{\text{crash}} = 0.963$

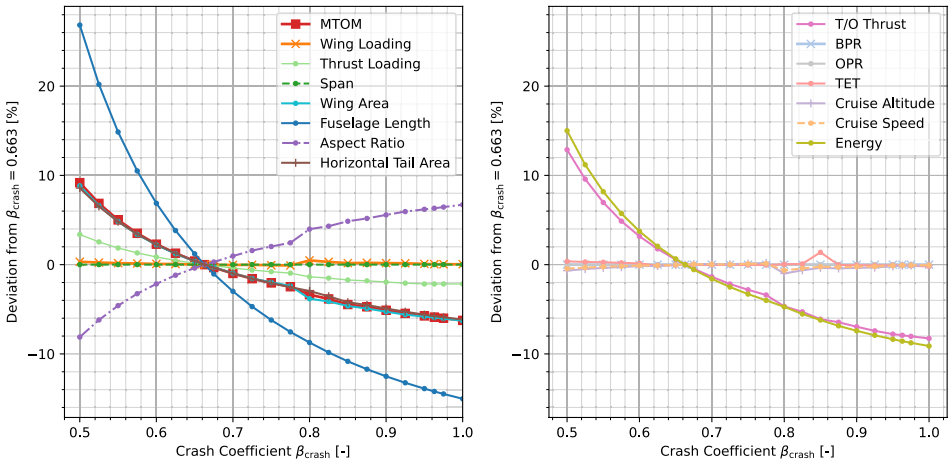

Fig. 5 Deviations of MED BASE aircraft with respect to that at $\beta_{\text{crash}} = 0.663$

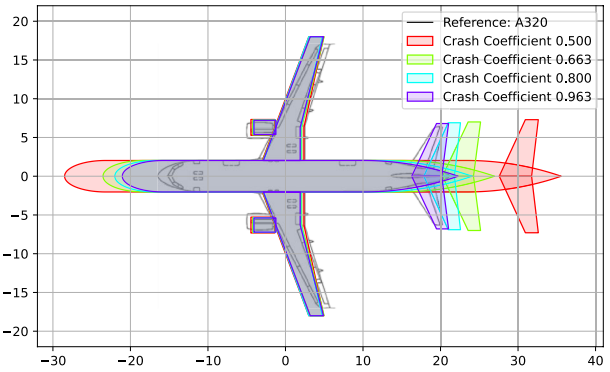

Fig. 6 Top view for MED BASE aircraft for different crash coefficients. The x-axis is such $x = 0$ at the quarter-chord of the mean aerodynamic chord. The A320 top-view [31] is shown for reference

Compared to the medium-range aircraft, the effect of crashworthiness is significantly reduced; notice that the fuselage length increases only by around 34% compared to 48% at $\beta_{\text{crash}} = 0.500$, whilst the MTOM increases by 4% for the regional aircraft compared to 6% for $\beta_{\text{crash}} = 0.663$.

These differences between the MED BASE and REG BASE aircraft are caused by the relative length of the baseline tank to the fuselage length. At $\beta_{\text{crash}} = 0.963$, the ratio of tank length to fuselage length is $6\ \text{m}/44\ \text{m} = 0.136$ for the MED aircraft, which is larger compared to $4.5\ \text{m}/40\ \text{m} = 0.112$ for the REG aircraft. This means that the tank, relative to the fuselage, is longer for the MED aircraft than the REG aircraft. The larger the ratio, the more sensitive the aircraft will be to changes in β_{crash}.

Table 6 OEM mass breakdown for MED BASE for different crash coefficients

β_{crash}	Component mass [metric tons (% OEM)]					OEM [metric tons]
	Fuselage	Wing	Engines	Empennage	H_2 tank	
0.500	15.8 (30.5 %)	8.8 (17.1 %)	7.7 (14.9 %)	1.1 (2.2 %)	1.7 (3.3 %)	51.7
0.663	11.9 (26.0 %)	8.4 (18.2 %)	6.9 (15.0 %)	1.1 (2.4 %)	1.5 (3.2 %)	46.0
0.800	10.6 (24.2 %)	8.1 (18.5 %)	6.5 (14.9 %)	1.1 (2.4 %)	1.4 (3.1 %)	43.9
0.963	9.5 (22.4 %)	8.0 (19.0 %)	6.4 (15.0 %)	1.0 (2.5 %)	1.3 (3.1 %)	42.3

Fig. 7 Deviations of REG BASE aircraft with respect to that at $\beta_{\text{crash}} = 0.963$

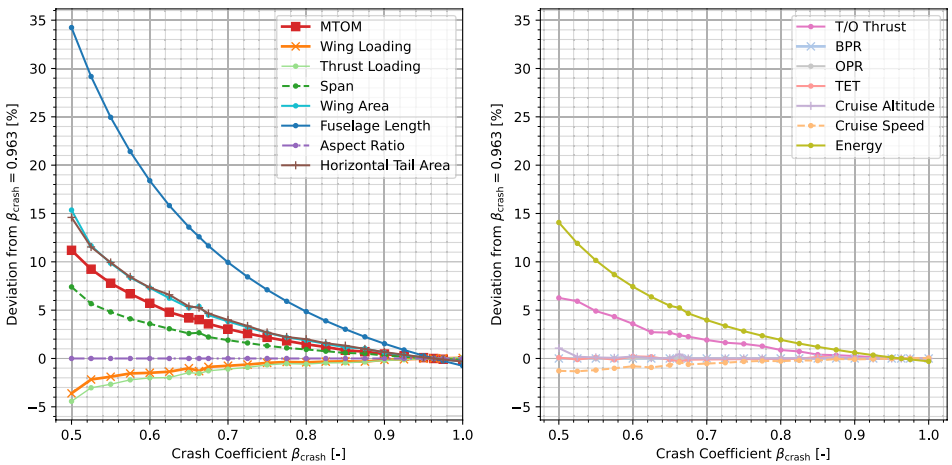

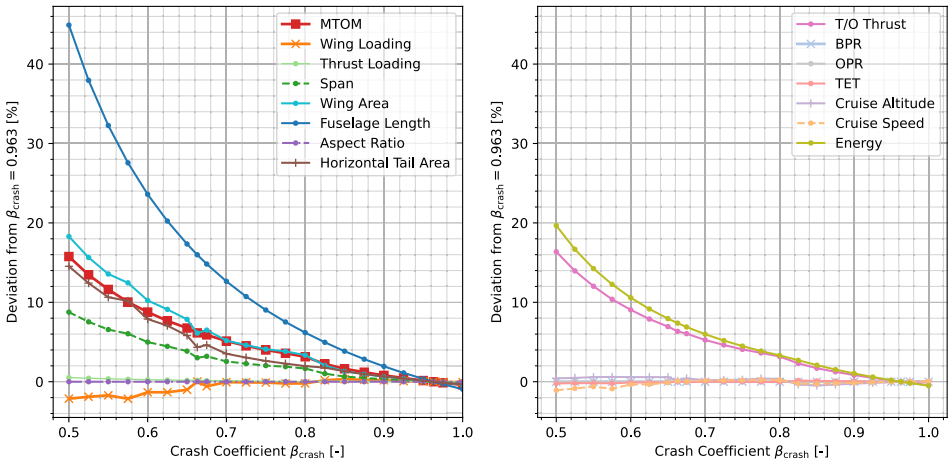

Fig. 8 Deviations of MED SPAN aircraft with respect to that at $\beta_{\text{crash}} = 0.963$

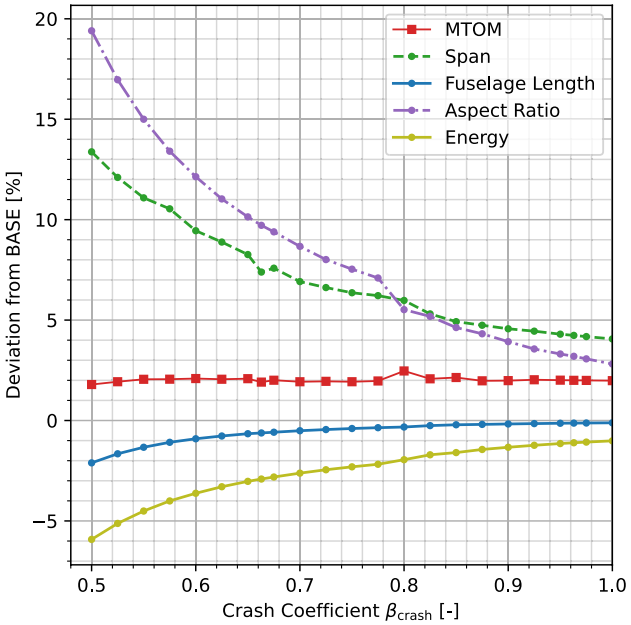

Fig. 9 Relative deviations of MED SPAN aircraft with respect to MED BASE aircraft, for every β_{crash}

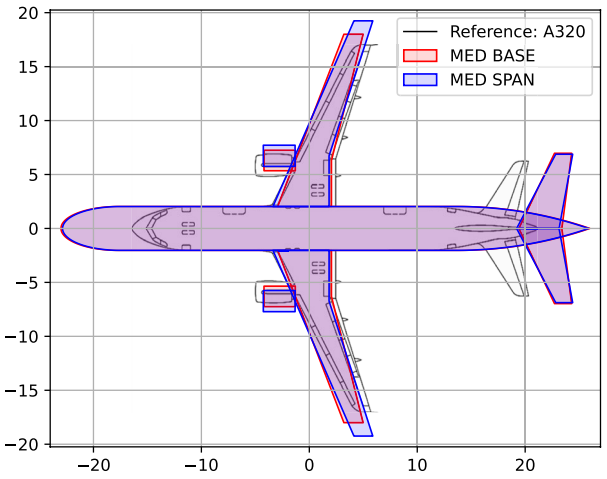

Fig. 10 MED BASE and MED SPAN aircraft top view for $\beta_{\text{crash}} = 0.700$, overlayed on top of A320 fuselage [31]

Overall, these results already answer the research question posed in the introduction; the performance of the aircraft is very sensitive to different crashworthiness capabilities of the fuselage structure, especially with respect to the fuselage length, fuel volume, and MTOM. The following sections address different ways the trends can be improved.

4.2 SPAN aircraft

For the MED BASE scenario, it is seen that the maximum span is a limiting factor. This section aims to discuss the effect of relaxing the span constraint. Figure 8 shows the tendencies of β_{crash} with respect to the $\beta_{\text{crash}} = 0.963$ case. It can be seen that the wing aspect ratio is now at its upper bound for all designs; the numerical value is increased compared to the MED BASE case. Similarly to the REG BASE aircraft, the optimizer chooses to decrease the wing loading for smaller crashed diameter coefficients. The thrust-loading remains invariant in spite of the change in wing loading because the OEI approach constraint is active. Figure 9 shows the elementwise comparison between the SPAN and BASE cases for every crash coefficient. Here it can be seen that the decrease in fuselage length is very limited, only at 1% for the $\beta_{\text{crash}} = 0.600$ case. The increase in wing aspect ratio causes a reduction in mission energy by around 2%, which reduces the fuel mass by the same amount. However, the increase in wing aspect ratio also increases the wing mass. The combination of these two effects cause the MTOM of the MED SPAN aircraft to be around 2% larger than the MED BASE case for any β_{crash}. Graphically, for $\beta_{\text{crash}} = 0.700$, the different aircraft geometries are plotted in Fig. 10.

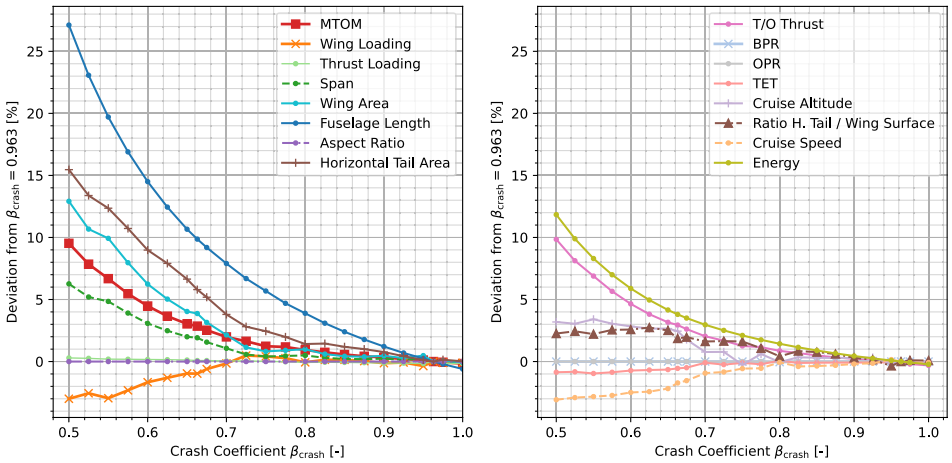

Fig. 11 Deviations of REG OVER aircraft with respect to that at $\beta_{\text{crash}} = 0.963$

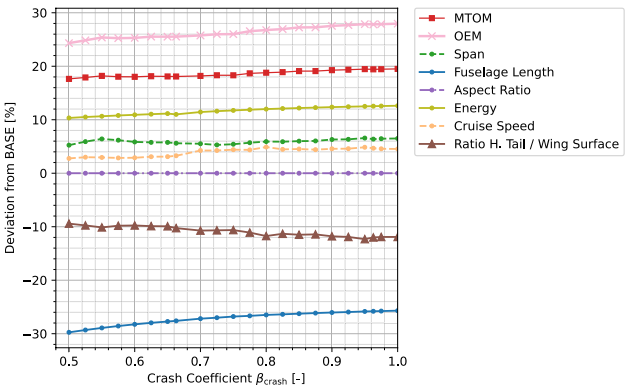

Fig. 12 Deviations of REG OVER aircraft from REG BASE aircraft, for every β_{crash}

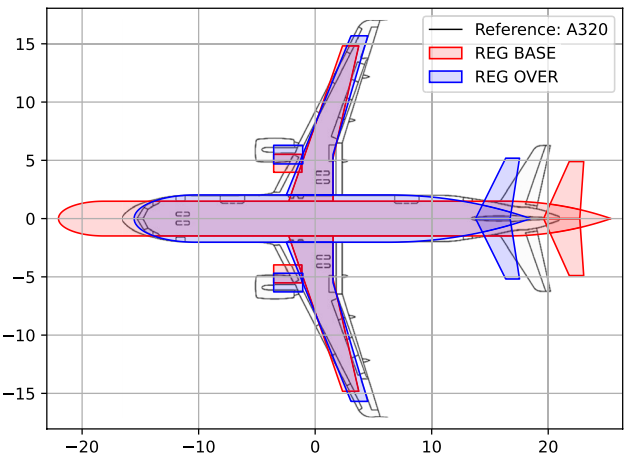

Fig. 13 REG BASE and REG OVER aircraft top view for $\beta_{\text{crash}} = 0.600$, overlayed on top of A320 fuselage [31]

4.3 OVER aircraft

Increasing the number of seats abreast can be a possible solution to aircraft with small crashed diameter coefficients and long fuselages. In this study, this is modeled via the 'over-sized' option; having a MED aircraft perform the mission of a REG aircraft, as explained in subsection 2.4. By increasing the number of seats abreast the effect is twofold. Firstly, the fuselage length is automatically reduced due to a smaller cabin length. The actual percentage reduction is a function of the number of passengers and the initial number of seats abreast. The reduction in fuselage length and increase in fuselage diameter reduce the fuselage's slenderness ratio, which affects the drag and weight contributions of the fuselage. Secondly, larger fuselage diameters allow for larger absolute crushing distances for the same crashed diameter coefficient, or alternatively, a larger crashed diameter coefficient for the same crushing distance.

The results of the optimizations for the REG OVER aircraft are shown in Fig. 11, and compared in Fig. 12 to the REG BASE aircraft in an elementwise fashion. Although the trends are similar to the that of BASE aircraft, there are notable differences that ought to be discussed.

Firstly, it can be seen that the fuselage length increases at a lower rate compared to the REG BASE aircraft; at $\beta_{\text{crash}} = 0.500$, the percentage difference compared to $\beta_{\text{crash}} = 0.963$ is 27% for the OVER case compared to 34% for the BASE case. As discussed in subsection 4.1 this is thought to be due to the relative length of the baseline tank to the fuselage length. In Fig. 12 it can be seen that converting an aircraft from the BASE type to OVER type results in a decrease of around 28% in fuselage length, albeit an increase in 19% and 11% in MTOM and mission energy, respectively. These results are independent on the crash coefficient. Similar to the REG BASE scenario, the wing aspect ratio is at the upper bound for REG OVER aircraft. The decrease in fuselage length can be better visualized in Fig. 13.

An important difference can be observed on Fig. 11. It appears that $\beta_{\text{crash}} = 0.700$ is a threshold point, below which the optimizer chooses to decrease the wing loading and the cruise speed significantly. Similarly to the MED SPAN case, the thrust-loading is unaffected because the active constraint in the thrust-loading versus wing-loading diagram is the OEI approach condition. This explains the deviations of wing-area and span. It is interesting to note that the ratio of horizontal tail surface to wing surface increases slightly with decreasing crash diameter coefficient. This could be due to the increase in $C_{L,\max}$, from the decrease in cruise speed (via the sweep angle). An increasing $C_{L,\max}$ requires a larger tail to trim the aircraft in landing, or in other words, the controllability performance is negatively affected. However, the horizontal tail surface to wing surface ratio is lower in REG OVER aircraft compared to REG BASE aircraft (refer to Fig. 12). This is due to a smaller c.g. range in over-sized aircraft, mainly attributed to the fewer number of passenger rows (smaller cabin length), and to a lesser extent to the smaller tank length and larger MTOM.

It can be concluded that increasing the seat abreast is an effective way of decreasing the length of the fuselage, at the cost of a heavier aircraft that is more fuel consuming.

4.4 DPAY aircraft

Another way of altering the effect of β_{crash} is by changing the design payload. The results of the optimizations when varying both the coefficient β_{crash} and the payload factor f_{pay} are shown in Fig. 14. The vertical axes of the graph can be changed to any variable of interest. For the purpose of this study, the length of the fuselage and MTOM are assessed. The latter is the parameter most sensitive to β_{crash}, while the former is an important design parameter. The graphs can be interpreted as follows. When moving vertically, the crash coefficient and the variable of interest vary, while the payload remains fixed; when $f_{\text{pay}} = 1$, the results are identical to the MED BASE case. Moving along the level curve involves keeping the crash coefficient constant while adjusting the payload and plotted variable accordingly. More interestingly, moving horizontally involves varying the payload and the crashed diameter coefficient while keeping the variable of interest fixed.

Suppose an aircraft is originally designed for a crashed diameter coefficient of 1.000, but the fuselage is discovered to perform at a $\beta_{\text{crash}} = 0.650$. Furthermore, consider that the aircraft is to be redesigned by reducing the payload to allow more space for the tank. To keep the same fuselage length, by following the red line in Fig. 14a, it can be seen that a reduction of 22% in payload is needed. To keep the MTOM constant, only 10% of payload needs to be removed. More importantly, this figure shows how expensive a redesign could have been when crashworthiness is not considered already during the preliminary design.

4.5 DRANG aircraft

Similarly to the previous section that focused on the payload, the design range can also influence the effect of the crashed diameter coefficient. As explained in subsection 2.4, the hydrogen tank is sized for the ferry range. In this study, as the design range is changed, the ferry range is reduced proportionally such that $r_{\text{ferry}}/r_{\text{des}}$ remains constant. The results can be seen in Fig. 15, and can be interpreted in the same way as Fig. 14, as explained in subsection 4.4.

Compared to the case of changing payload requirement, it can be observed that the slope of the level curves

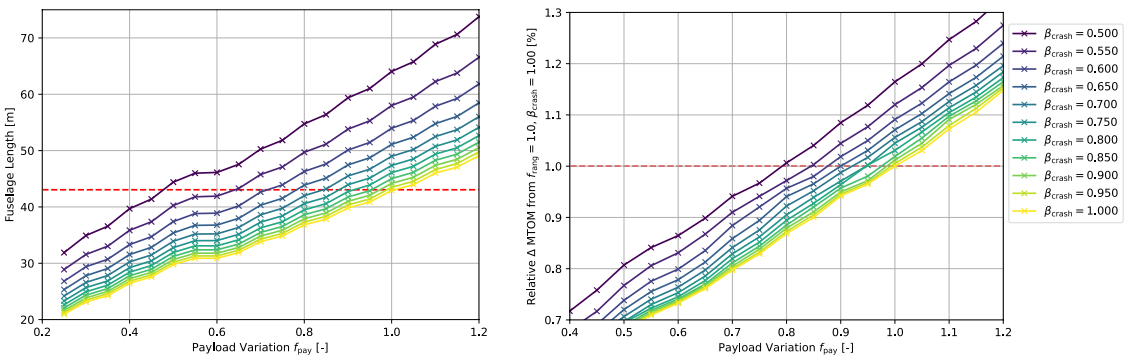

(a) Effect on fuselage length.

(b) Effect on MTOM, relative to $\beta_{\text{crash}} = 1.000$ and $f_{\text{pay}} = 1.00$.

Fig. 14 Effect of changing the design payload and crash coefficient for a MED aircraft. The red line in both figures coincides with the aircraft with $\beta_{\text{crash}} = 1.000$ and $f_{\text{pay}} = 1.00$

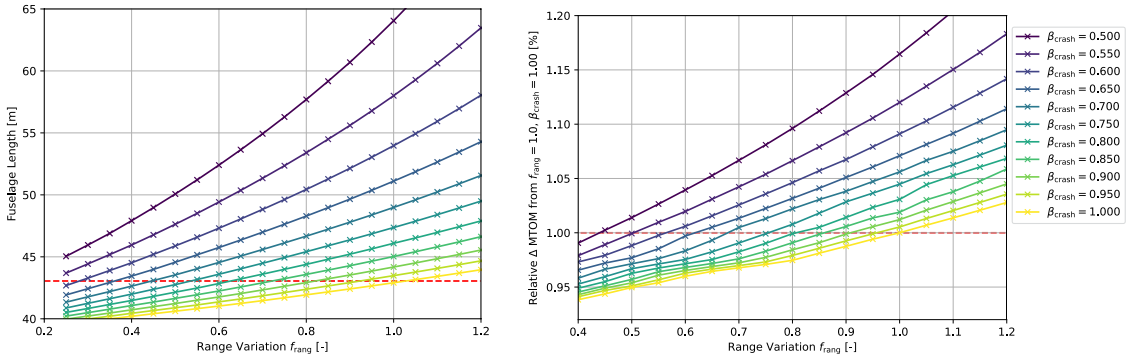

(a) Effect on fuselage length.

(b) Effect on MTOM, relative to $\beta_{\text{crash}} = 1.000$ and $f_{\text{rang}} = 1.00$.

Fig. 15 Effect of changing the design range and crash coefficient for a MED aircraft. The red line in both figures coincides with the aircraft with $\beta_{\text{crash}} = 1.000$ and $f_{\text{rang}} = 1.00$

of β_{crash} is smaller, meaning that the plotted variables (fuselage length and MTOM) are less sensitive to changes in range requirement. Suppose again that an aircraft is designed for $\beta_{\text{crash}} = 1.000$, but later in the design it is discovered that the fuselage performs at $\beta_{\text{crash}} = 0.750$. If a redesign is made such that the design range is varied as described above, whilst keeping the fuselage length constant, the design range needs to be decreased by around 50%! If the MTOM wants to be conserved instead, the design range must be reduced by 25%. A smaller slope requires one to shift further to the left to keep the parameter of interest constant.

The reason behind the smaller slope and the asymptotic behavior in the range plots compared to the payload plots is due to the (lack of) variation in cabin length. When the payload is reduced, both the cabin length and the tank length are reduced, which together significantly change the fuselage length. On the other hand, when the range is reduced, the reduction in fuselage length is only due to the decrease of tank length. Hence, in the limit as the tank length goes to zero, the fuselage length approaches a constant value because the cabin length doesn't change. This explains both the asymptote and the smaller slope.

Furthermore, referring back to the discussion of subsection 4.1 with the ratio of tank length to fuselage length to explain the sensitivity of aircraft performance parameters to changes in crash coefficient, when the payload is varied, this ratio remains fairly constant. This can be seen in Fig. 14 with lines of constant β_{crash} being parallel. However, when the range is reduced, the ratio of tank length to fuselage length decreases, implying that the aircraft is less sensitive to changes in β_{crash}. This is seen in Fig. 15; as f_{rang} is reduced, the difference between the line of $\beta_{\text{crash}} = 0.500$ and that of $\beta_{\text{crash}} = 1.000$ reduces.

4.6 Limitations

It is important to discuss the limitations of the present study, and how this influences the above results;

1. *Scrape angle concerns.* Proesmans and Vos' framework [28] assumes the landing gear is attached to the wing, but does not consider the scrape angle as a criterion for wing placement. Low crash coefficients yield extremely long aircraft, and to comply with the scrape angle the wing needs to be positioned further aft, which requires a larger tail and snowballs into a heavier aircraft. This was studied by Manzano [34].
2. *Fuselage mass.* The crashworthiness structure that would ensure a given crash coefficient has not been accounted for in the mass of the fuselage. Furthermore, when the fuselage length is large due to a low crash coefficient, its Class-II weight estimation based on similar aircraft becomes less applicable. Therefore, the fuselage mass is underestimated in this study, and accounting for the crashworthiness structure would only worsen the snowball effect.
3. *High surface area-to-volume for low crash coefficients.* When the crash coefficient is low, the length of the tank becomes several times larger than its diameter. If it were a single tank, it would be thermodynamically less efficient at maintaining a low temperature, so hydrogen would boil-off at a higher rate [3]. Boil-off is already not accounted for in the $f_{V,\text{extra}}$, but this greater hydrogen loss is much more significant for lower crash coefficients and may be non negligible. On the contrary, if the tank were to be split into smaller tanks to reduce boil-off and single-point-failures, its increase in mass has also not been accounted for. Both of these arguments also suggest

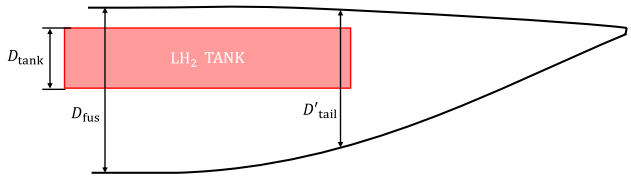

Fig. 16 Example of increased effective crash coefficient in tailcone

that η_{tank} is not independent on the crash coefficient; its relationship is left as a recommendation.

4. *Vertical positioning of the tank.* The vertical positioning of components is not analyzed in the framework, but effect of the crashed diameter coefficient with long tanks for small β_{crash} would influence the moment of inertia, and hence the dynamic response of the aircraft.
5. *Tank not placed inside tail.* The length of the fuselage is computed as the sum of the cockpit length, cabin length, tank length and tail length. There is no attempt at reducing the fuselage length by placing part of the tank inside the tail segment. This would improve the trends observed in this study.
6. *Increased effective crashed diameter coefficient in the tailcone.* When the hydrogen tank extends into the tailcone, if the diameter of the tank is unaltered, the crushing distance below the tank is reduced. This implies a larger effective β_{crash} than that designed for a section of maximum fuselage diameter. This can be seen in Fig. 16, where $D'_{\text{tail}} < D_{\text{fus}}$. To evaluate if this detail is important, the actual crash dynamics need to be studied, which is deemed outside the scope of the research. These considerations have not been accounted for; it is the maximum fuselage diameter that is used to size the tank via the crash coefficient, as explained in subsection 2.3.

5 Sensitivities

Given the modifications on the hydrogen tank geometry due to the crash coefficient, it is important to review the assumptions involved with the mass and geometry of the tank via the gravimetric index, the extra volume allowance

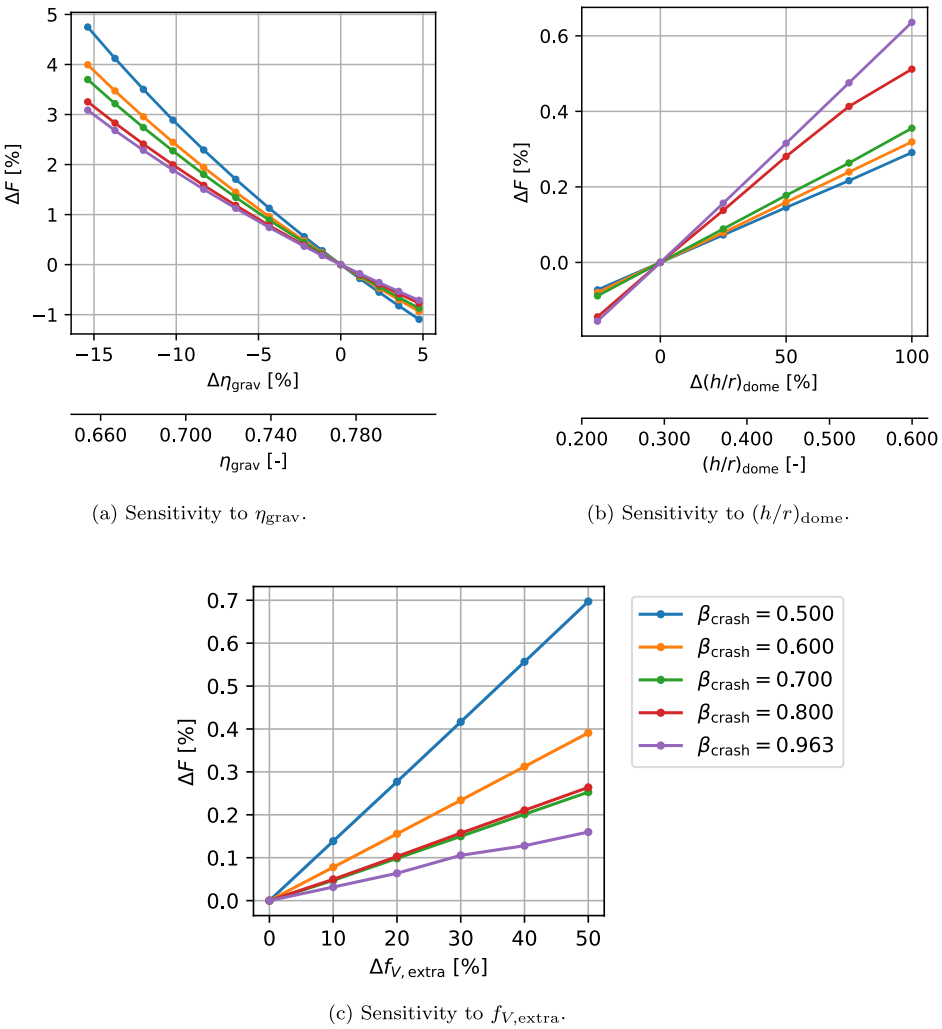

Fig. 17 Sensitivity of the objective function, mission energy, with respect to hydrogen tank parameters for an energy-optimal MED BASE aircraft

(a) Sensitivity to η_{grav}.

(b) Sensitivity to $(h/r)_{\text{dome}}$.

(c) Sensitivity to $f_{V,\text{extra}}$.

and the geometry of the tank domes. This has already been discussed by Proesmans [28], but for cost-optimal aircraft, without the influence of the crashed diameter coefficient.

Figure 17a shows how a reduction in crash coefficient makes the objective function more sensitive to changes in gravimetric index, in the order of 2%. This is explained by the larger tanks that are required for smaller crash coefficients; changes in mass are more significant.

In Fig. 17b a decreasing β_{crash} causes the mission energy to be less sensitive to changes in gravimetric index. Similarly to the gravimetric index, as β_{crash} is lowered, the tank becomes longer, and changes in the dome height have a smaller effect on the total volume capacity of the tank.

Finally, in Fig. 17c it can be seen that a smaller β_{crash} significantly increases the sensitivity of the mission energy on the extra volume allowances, by a factor up to 4. For smaller β_{crash} values, larger volume allowances are associated with even longer tanks, which snowballs into a more fuel consuming aircraft. As a follow up to limitation number 3, described in subsection 4.6, it is left as a recommendation to identify the volume allowance equivalent to modeling boil-off in the tank for small values of β_{crash}. An approach as implemented by [18] could be used for this. It is seen that the line of $\beta_{\text{crash}} = 0.800$ is shows more sensitivity to that of $\beta_{\text{crash}} = 0.700$; this is thought to be an anomaly and is left for further study.

6 Conclusion and recommendations

The objective of this research is to quantify the effect of the crashed diameter coefficient on aircraft design by performing multidisciplinary design optimizations of energy-optimal aircraft and comparing solutions of different crash coefficients. It is found that, for the same payload and range requirements, accounting for the coefficient increases the fuselage and maximum take-off mass by around 17% and 6%, respectively for a short/medium-range aircraft type. For a regional aircraft, the effect is much less pronounced, increasing the fuselage length and maximum take-off mass by approximately 13% and 4%, respectively.

Increasing the span limit has limited influence on the tendencies. The improvement in fuel consumption is absorbed by the increase in maximum take-off mass, yielding similar fuselage lengths overall. On the other hand, the 'oversized' option that increases the number of seats abreast is very beneficial to reduce the fuselage length by 27%, but with the drawback of 19% larger MTOM and 11% mission energy. However, when looking at the absolute area available for a crash structure, such a consideration might be interesting.

It is found that the MTOM and fuselage length are more sensitive to changes the payload requirement than changes in the range requirement. If the fuselage length is kept constant, and the crashed diameter coefficient is reduced from 1.000 to 0.663 (the A320 fuselage value), either the payload requirement is reduced by at least 20%, or the design range is reduced by at least 50%, under the assumption that the ferry range is reduced proportionally.

The limitations of this study lie primarily in the fact that the wing placement is not adjusted according to the scrape angle and that a non-conservative estimation of the fuselage mass is used which does not account for the added mass of the crashworthy structures. Incorporating these changes would only exacerbate the existing trends, and is left as a recommendation to study. Furthermore, structural sizing for varying crash coefficients is another interesting follow-up research topic. On the other hand, the wing aspect ratio was limiting in several optimizations. The effect of increasing the upper bound could also be considered, provided that appropriate wing weight estimations for these high aspect ratios allow. Furthermore, the study can be extended to consider long-range aircraft (although, as illustrated in [18], these aircraft already suffer from dramatic increases in fuselage length in a LH_2 version), as well as other seat-abreast configurations or continuous variations in the fuselage diameter (although the current results and other studies [18] suggest that benefits are unlikely). Similarly, the effects of optimizing for cost and climate, instead of energy is left as a recommendation. Also, a follow-up study could be conducted on the relationship between the tank gravimetric index and the crash coefficient.

Overall, the effect of crashworthiness in the design of hydrogen aircraft has been confirmed to be significant. If unaccounted for in preliminary design, the consequences can be disastrous.

Appendix

Constraint diagrams

This appendix presents the constraint diagram in the form of thrust-loading versus wing-loading of the MED BASE (Fig. 18) and REG BASE (Fig. 19) aircraft, for crashed diameter coefficients $\beta_{\text{crash}} = 0.963$ and $\beta_{\text{crash}} = 0.500$.

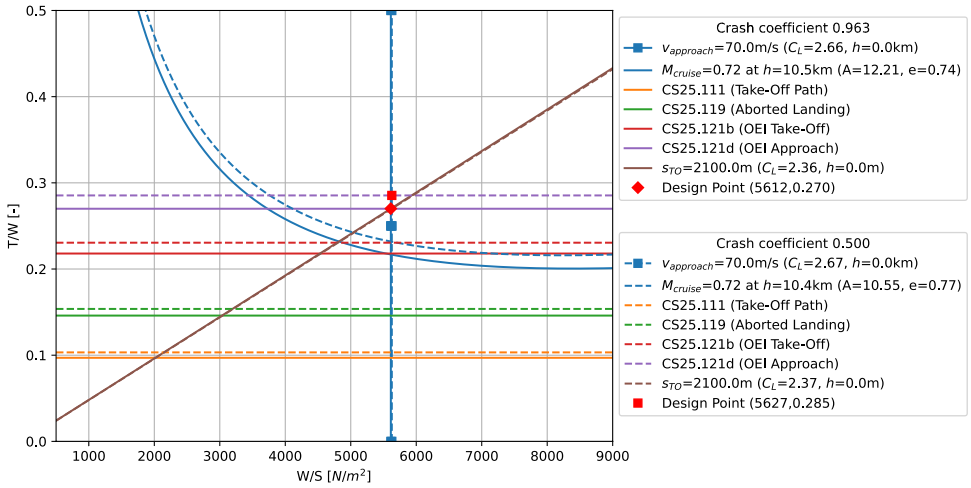

Fig. 18 Constraint diagram for MED BASE aircraft

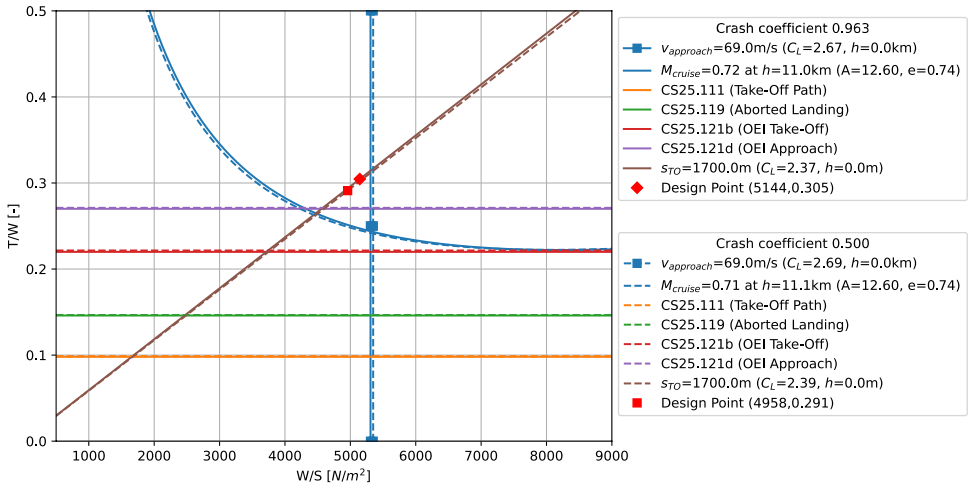

Fig. 19 Constraint diagram for REG BASE aircraft

Acknowledgements This research is conducted within the research and innovation programme "Luchtvaart in Transitie", which is funded by the Dutch National Growth Fund (Groeifonds). It is part of the "H2Crash" project, and part of The CrashProof Knowledge Centre (CrashProofLab) [35].

Author contributions A.M.M. wrote the main manuscript text and developed the entire methodology. S.C. conceptualized the study and supervised the crashworthiness part. M.H. and P.P. supervised the aircraft design part. All authors participated in revising and editing the manuscript to its present version.

Data availability No datasets were generated or analysed during the current study.

Declarations

Conflict of interest The authors declare no conflict of interest.

References

1. Lee, D., Fahey, D., Skowron, A., Allen, M., Burkhardt, U., Chen, Q., Doherty, S., Freeman, S., Forster, P., Fuglestvedt, J., Gettelman, A., De León, R., Lim, L., Lund, M., Millar, R., Owen, B., Penner, J., Pitari, G., Prather, M., Sausen, R., Wilcox, L.: The contribution of global aviation to anthropogenic climate forcing for 2000 to 2018. Atmos. Environ. **244**, 117834 (2021). https://doi.org/10.1016/j.atmosenv.2020.117834
2. Owen, B., Lee, D.S., Lim, L.: Flying into the future: Aviation emissions scenarios to 2050, (2010). https://doi.org/10.1021/es902530z
3. Adler, E.J., Martins, J.R.: Hydrogen-powered aircraft: Fundamental concepts, key technologies, and environmental impacts. Prog. Aerosp. Sci. **141**, 100922 (2023). https://doi.org/10.1016/j.paerosci.2023.100922
4. Verstraete, D.: On the energy efficiency of hydrogen-fuelled transport aircraft. Int. J. Hydrogen Energy **40**(23), 7388–7394 (2015). https://doi.org/10.1016/j.ijhydene.2015.04.055

5. Goldmann, A., Sauter, W., Oettinger, M., Kluge, T., Schröder, U., Seume, J.R., Friedrichs, J., Dinkelacker, F.: A study on electrofuels in aviation. Energies (2018). https://doi.org/10.3390/en11020392
6. Rao, A.G., Yin, F., Werij, H.: Energy transition in aviation: the role of cryogenic fuels. Aerospace **7**(12), 181 (2020). https://doi.org/10.3390/aerospace7120181
7. International Air Transport Association (IATA), Liquid Hydrogen as a Potential Low-Carbon Fuel for Aviation, https://www.iata.org/contentassets/d13875e9ed784f75bac90f000760e998/fact_sheet7-hydrogen-fact-sheet_072020.pdf, Jul. 2020. IATA Fact Sheet No. 7, July 2020
8. Westenberger, A., et al.: Liquid hydrogen fuelled aircraft-system analysis, CRYOPLANE, The European Commission, Brussels, Belgium, Report No. GRD1-1999-10014, (2003)
9. Wallington, T., Woody, M., Lewis, G., Keoleian, G., Adler, E., Martins, J., Collette, M.: Hydrogen as a sustainable transportation fuel. Renew. Sustain. Energy Rev. **217**, 115725 (2025). https://doi.org/10.1016/j.rser.2025.115725
10. Khandelwal, B., Karakurt, A., Sekaran, P.R., Sethi, V., Singh, R.: Hydrogen powered aircraft: The future of air transport. Prog. Aerosp. Sci. **60**, 45–59 (2013). https://doi.org/10.1016/j.paerosci.2012.12.002
11. Silberhorn, D., Atanasov, G., Walther, J.-N., Zill, T.: Assessment of Hydrogen Fuel Tank Integration At Aircraft Level. In: Proceedings of the Deutscher Luft- und Raumfahrtkongress, (2019)
12. Healy, F., Gu, H., Rezgui, D., Cooper, J.: Wing mounted hydrogen fuel tanks: mitigating the aeroelastic penalties of dry configurations? International Forum on Aeroelasticity and Structural Dynamics, The Hague, (2024)
13. Verstraete, D.: Long range transport aircraft using hydrogen fuel. Int. J. Hydrogen Energy **38**(34), 14824–14831 (2013). https://doi.org/10.1016/j.ijhydene.2013.09.021
14. Troeltsch, F.M., et al.: with Minimized Climate Impact, AIAA AVIATION,: FORUM. American Institute of Aeronautics and Astronautics **2020**,(2020). https://doi.org/10.2514/6.2020-2660
15. Nicolay, S., Karpuk, S., Liu, Y., Elham, A.: Conceptual design and optimization of a general aviation aircraft with fuel cells and hydrogen. Int. J. Hydrogen Energy **46**(64), 32676–32694 (2021). https://doi.org/10.1016/j.ijhydene.2021.07.127
16. Gao, Y., Jausseme, C., Huang, Z., Yang, T.: Hydrogen-powered aircraft: hydrogen–electric hybrid propulsion for aviation. IEEE Electrif. Mag. **10**(2), 17–26 (2022). https://doi.org/10.1109/mele.2022.3165725
17. Mukhopadhaya, J., Rutherford, D.: Performance analysis of evolutionary hydrogen-powered aircraft, International Council on Clean Transportation, (2022)
18. Onorato, G., Proesmans, P., Hoogreef, M.F.M.: Assessment of hydrogen transport aircraft: Effects of fuel tank integration. CEAS Aeronaut. J. **13**(4), 813–845 (2022). https://doi.org/10.1007/s13272-022-00601-6
19. Eissele, J., et al.: Hydrogen-powered aviation-design of a hybrid-electric regional aircraft for entry into service in 2040. Aerospace **10**(3), 277 (2023). https://doi.org/10.3390/aerospace10030277
20. Jagtap, S.S., Childs, P.R., Stettler, M.E.: Conceptual design-optimisation of a subsonic hydrogen-powered long-range blended-wing-body aircraft. Int. J. Hydrogen Energy **96**, 639–651 (2024). https://doi.org/10.1016/j.ijhydene.2024.11.331
21. Adler, E.J., Martins, J.R.R.A.: Blended wing body configuration for hydrogen-powered aviation. J. Aircr. **61**(3), 887–901 (2024). https://doi.org/10.2514/1.c037582
22. Proesmans, P., Vos, R.: Hydrogen, medium-range airplane design optimization for minimal global warming impact. CEAS Aeronaut. J. **15**(4), 781–806 (2024). https://doi.org/10.1007/s13272-024-00734-w
23. Simonetto, M., Pascoe, J.-A., Sharpanskykh, A.: Preliminary safety assessment of a liquid hydrogen storage system for commercial aviation. Safety **11**(1), 27 (2025). https://doi.org/10.3390/safety11010027
24. Schwinn, D.B.: Integration of crashworthiness aspects into preliminary aircraft design. Appl. Mech. Mater. **598**, 146–150 (2014). https://doi.org/10.4028/www.scientific.net/amm.598.146
25. Federal Aviation Administration, Hydrogen-Fueled Aircraft Safety and Certification Roadmap, Tech. Rep. AIR-241122-001, U.S. Department of Transportation, Federal Aviation Administration, Washington, DC, Dec. 2024. https://www.faa.gov/aircraft/air_cert/step/disciplines/propulsion_systems/hydrogen-fueled_aircraft_roadmap, accessed (29 July 2025)
26. Keijzer, D., Soria, C.S., Arends, J., Sarıgöl, B., Scarano, F., Castro, S.G.: Design of a Hydrogen-Powered Crashworthy eVTOL Using Multidisciplinary Analysis and Design Optimization. AIAA SCITECH 2024 Forum. (2024). https://doi.org/10.2514/6.2024-2474
27. LePage, F., Carciente, R.: A320 Fuselage Section Vertical Drop Test, Part 2: Test Results, Tech. rep., CEAT Test report S95 5776/2, (1995)
28. Proesmans, P., Vos, R.: Airplane design optimization for minimal global warming impact. J. Aircr. **59**(5), 1363–1381 (2022). https://doi.org/10.2514/1.C036529
29. Torenbeek, E.: The initial calculation of range and mission fuel during conceptual design, Tech. Rep. LR-525, Delft University of Technology, Faculty of Aerospace Engineering (1987)
30. Embraer, S.A.: Embraer 175 Airport Planning Manual, Tech. rep., Embraer S.A (2021)
31. Airbus S.A.S. Customer Services, Airbus A320 Aircraft Characteristics Airport and Maintenance Planning, Tech. rep., Airbus S.A.S. Customer Services, (2019)
32. Proesmans, P., Vos, R.: Comparison of future aviation fuels to minimize the climate impact of commercial aircraft, AIAA AVIATION 2022 forum. Am. Inst. Aeronaut. Astronaut. (2022). https://doi.org/10.2514/6.2022-3288
33. Virtanen, P., et al.: SciPy 1.0: fundamental algorithms for scientific computing in Python, Nature Methods, Vol. 17, No. 3, (2020), pp. 261–272. https://doi.org/10.1038/s41592-019-0686-2
34. Garmilla Manzano, A., Vos, R., Asaro, S., Fritzsche, F.: Systematic Tailplane Design for an Aircraft Family Concept. MSc, Thesis (2024)
35. Castro, S.: The CrashProof Knowledge Centre (CrashProofLab) (2022). https://doi.org/10.5281/zenodo.11500722